arXiv:1703.06560v1 [astro-ph.SR] 20 Mar 2017

Solar Filament Longitudinal Oscillations along a Magnetic Field Tube with Two Dips

Yu-Hao Zhou[1,2], Li-Yue Zhang[1,2], Y. Ouyang[1,2], P. F. Chen[1,2] and C. Fang[1,2]
[1] *School of Astronomy and Space Science, Nanjing University, Nanjing 210023, China;*
chenpf@nju.edu.cn
[2] *Key Laboratory of Modern Astronomy & Astrophysics (Nanjing University), Ministry of Education, Nanjing 210023, China*

ABSTRACT

The large-amplitude longitudinal oscillations of solar filaments have been observed and explored for more than ten years. Previous studies are mainly based on the one-dimensional rigid flux tube model with a single magnetic dip. However, it is noticed that there might be two magnetic dips, and hence two threads, along one magnetic field line. Following the previous work, we intend to investigate the kinematics of the filament longitudinal oscillations when two threads are magnetically connected, which is done by solving one-dimensional radiative hydrodynamic equations with the numerical code MPI-AMRVAC. Two different types of perturbations are considered, and the difference from previous works resulting from the filament thread-thread interaction is investigated. We find that even with the inclusion of the thread-thread interaction, the oscillation period is modified weakly, by at most 20% compared to the traditional pendulum model with one thread. However, the damping timescale is significantly affected by the thread-thread interaction. Hence, we should take it into account when applying the consistent seismology to the filaments where two threads are magnetically connected.

Subject headings: Sun: filaments, prominences - Sun: oscillations - methods: numerical

1. Introduction

As one type of solar activity, filaments (or prominences) are a relatively long-lived phenomenon (Tandberg-Hanssen 1995). Unlike solar flares, which last for only tens of minutes, solar filaments, except some dynamic active-region filaments, can survive for days or weeks (Engvold 2004). Although some of them might be due to continual flows of chromospheric plasma along magnetic field lines where magnetic dips are not required (Wang & Sheeley 1999; Karpen et al. 2001; Zou et al. 2016, 2017), most filaments are believed to be supported by magnetic dips, whose upward Lorentz force compensates for the gravity (Kippenhahn & Schlüter 1957; Arregui et al. 2012). During the long lifetime, it is inevitable for the filament to be disturbed by a nearby flare (Jing et al. 2003) or incoming shock waves (Shen et al. 2014). As a result, the filament would then oscillate with a large amplitude. The shaking of the footpoints of the magnetic field lines can induce propagating Alfvén waves (Erdélyi & Fedun 2007), and hence lead to small-amplitude longitudinal oscillations of the filament threads, which can account for the counterstreamings of the filaments (Chen et al. 2014).

Filament oscillations have been observed for decades since they were identified by the winking appearance (Ramsey & Smith 1966). Winking filaments are visible only when the oscillation velocity is large, say, larger than 20 km s^{-1}(Oliver et al. 2002). These large-amplitude oscillations are generally believed to be transverse ones. Later, spectral observations with higher resolutions discovered filament oscillations with small amplitude down to 500 m s^{-1} (Zhang & Engvold 1991). In theory, these os-

cillations are modeled by different eigen modes (Joarder & Roberts 1992a,b), which provides the foundation for prominence seismology (Soler et al. 2010), and magnetic parameters can be derived accordingly (Arregui et al. 2012).

In 2003, a new type of filament oscillations was discovered, which are manifested as the monolithic oscillations of the threads along the thread direction (Jing et al. 2003). Since it is believed that filament threads trace the local supporting magnetic field lines, this type of oscillation is called large-amplitude longitudinal oscillations (Jing et al. 2003; Vršnak et al. 2007), in contrast to the small-amplitude longitudinal oscillations (Bashkirtsev et al. 1983). Several mechanisms were qualitatively proposed to explain the restoring force for such oscillations, e.g., the field-aligned component of gravity, pressure gradient, and magnetic tension force or pressure force (Jing et al. 2003; Vršnak et al. 2007; Li & Zhang 2012). With the geometry of the magnetic field line taken from observations, Zhang et al. (2012) performed 1-dimensional (1D) radiative hydrodynamic simulations of a filament thread. Their simulations reproduced the oscillation period, though the resulting damping time is longer than that in observations. Noticing that the gas pressure gradient is much smaller than the gravity, they concluded that the field-aligned component of gravity is the restoring force for the longitudinal oscillations. With a parameter survey, Luna & Karpen (2012) verified that except for the case with extremely shallow dips, the field-aligned component of gravity generally overwhelms the gas pressure gradient inside the coronal loop, suggesting that the gravity is the main restoring force. Therefore, the large-amplitude longitudinal oscillations are considered as the pendulum mode (Luna et al. 2012). Within such a framework, Zhang et al. (2013) conducted a parameter survey with radiative hydrodynamic simulations, by which they derived empirical formulae to relate the oscillation period and damping timescale to the geometric parameters of the magnetic dip and the perturbation velocity.

It should be pointed out that all of these numerical simulations are based on the assumption that the filament threads are totally independent, and only one dip is present along one magnetic field line. However, some of the magnetic field lines may possess more than one dip. For example, Mackay & van Ballegooijen (2009) studied the effect of a small magnetic element approaching a solar filament through nonlinear force-free modeling. It is found that some field lines have double dips although the twist of the field line is less than one turn. The nonlinear force-free field extrapolation conducted by Jing et al. (2010) also shows the existence of double dips in some field lines. Moreover, double dips are a natural result for some field lines in the head-to-tail model for the filament formation (Martens & Zwaan 2001). In the case of double dips along one magnetic flux tube, the filament threads on the double dips would interact with each other when oscillating.

From observational point of view, it has been revealed that multiple threads in one filament oscillate in unison (Yi et al. 1991; Terradas et al. 2002; Lin et al. 2007), indicative of interactions among individual threads. Such an interaction between two adjacent threads is analytically and numerically investigated by Díaz et al. (2005) and Díaz & Roberts (2006). These works focus on the transverse mode of the filament oscillations, where different threads interact through fast-mode magnetoacoustic waves. Fast-mode waves might also be excited in filament longitudinal oscillations if the magnetic field is so weak that the heavy filament thread moving along the field line can alter the magnetic field line (Li & Zhang 2012). However, when the magnetic field is strong, filament longitudinal oscillations can excite only the slow-mode waves, which propagate along the field line. In this case, when there are two magnetic dips that host two threads, the two threads would also interact through slow-mode waves. It is of great interest to see how the interaction between the magnetically connected two threads affects their oscillation behaviors during a longitudinal oscillation. In this paper, we aim to investigate the large-amplitude longitudinal oscillations of double threads along one flux tube. The paper is arranged as follows. The numerical setup is described in Section 2, and the results are presented in Section 3, which are followed by discussions in Section 4.

2. Numerical Method

Following previous research, we perform 1D radiative hydrodynamic simulations to study the longitudinal oscillations of solar filaments, where

the deformation of the magnetic flux tube and the variation along the flux tube are ignored. This seems to be a quite reasonable approximation since the 2-dimensional simulations performed by Luna et al. (2016) revealed that there are no obvious interactions between threads in different field lines during longitudinal oscillations. The 1D radiative hydrodynamic equations used in this paper are as follows:

$$\frac{\partial \rho}{\partial t} + \frac{\partial}{\partial s}(\rho v) = 0, \tag{1}$$

$$\frac{\partial}{\partial t}(\rho v) + \frac{\partial}{\partial s}(\rho v^2 + p) = \rho g_{\parallel}(s), \tag{2}$$

$$\frac{\partial E}{\partial t} + \frac{\partial}{\partial s}(Ev + pv) = \rho g_{\parallel} v - n_e n_H \Lambda(T) + \frac{\partial}{\partial s}(\kappa \frac{\partial T}{\partial s}) + H(s), \tag{3}$$

where s is the distance along the rigid flux tube, $g_{\parallel}(s)$ is the field-aligned component of the gravity, and all the rest symbols in the equations have their usual meanings. With the contributions from hydrogen and helium, the mass density ρ is related to the number density by $\rho = 1.4 m_p n_H$, and the gas pressure is $p = 2.3 n_H k_B T$. The total energy $E = \rho v^2/2 + p/(\gamma - 1)$, where $\gamma = 5/3$ is the adiabatic index. The right-hand side of equation (3) includes optically thin radiative (the second term), heat conduction (the third term) and an additional volumetric heating term (the last term). $\Lambda(T)$ is the radiative loss coefficient, whose distribution can be found in Figure 1 of Xia et al. (2011). $\kappa = 10^{-6} T^{5/2}\,\mathrm{erg\,cm^{-1}\,s^{-1}\,K^{-1}}$ is the Spitzer-type heat conductivity. The steady background heating term $H(s)$, which is expressed below, is applied to maintain the hot corona:

$$H(s) = \begin{cases} E_0 \exp\left(-s/H_m\right), & s < L/2; \\ E_0 \exp[-(L-s)/H_m], & L/2 \le s < L. \end{cases} \tag{4}$$

The heating rate decays exponentially with the distance, with the base amplitude being $E_0 = 3 \times 10^{-4}\,\mathrm{erg\,cm^{-3}\,s^{-1}}$ (Withbroe & Noyes 1977). The scale length is taken to be $H_m = L/2$ (Withbroe 1988). This heating is based on the assumption that the energy of the background heating originates from the photospheric motions (Aschwanden & Schrijver 2002).

Note that $g_{\parallel}(s)$ in equation (2) is determined by the shape of the flux tube. Following Xia et al. (2011), the flux tube is composed of several parts: A vertical part with a length of $s_1 = 5$ Mm and a quarter-circle with a length of s_2=15.7 Mm at each leg of the field line, and a central part at the top, as illustrated by Figure 1(a). In the case of one dip, the shape of the central part is generally described by a cosine function (Xia et al. 2011; Zhang et al. 2013). In order to get two dips, we use a helix with two turns. The curve of the helix is described by the following formulae in the local coordinates,

$$\begin{cases} x = (\theta/4\pi)^n l; \\ y = 0.5 D \sin\theta; \\ z = 0.5 D \cos\theta; \end{cases} \tag{5}$$

where x is the horizontal axis along the main axis of the helix, y is the horizontal axis perpendicular to x, and the z-axis is upward, D is the depth of the dips, l is the axial length of the helix, and θ ranges from 0 to 4π. The parameter n controls the shapes of the two dips. When $n = 1$, the two dips are identical. As shown in Figure 1(a), the two dips have a length of w_1 and w_2, respectively, with $w_1 + w_2 = l$. If $n > 1$, then w_2 is larger than w_1. The helix is viewed from another angle in Figure 1(b). In this paper, $D = 3$ Mm is chosen, similar to previous research (Antiochos et al. 1999, 2000; Karpen et al. 2005, 2006; Zhang et al. 2012). Of course, there can be many other types of non-uniform helixes with different geometric parameters. However, as pointed out by Luna & Karpen (2012) and Zhang et al. (2013), the oscillation period is mainly controlled by the curvature radius of the magnetic dip. In this paper, the curvature radius changes as l changes. Once the geometry of the flux tube is determined, we can derive $g_{\parallel}(s)$ by $\boldsymbol{g} \cdot \hat{\mathbf{e}}_{\mathbf{s}}$, where $\boldsymbol{g} = -274 \hat{\mathbf{e}}_{\mathbf{z}}$ m s^{-2}, $\hat{\mathbf{e}}_{\mathbf{z}}$ is the unit vector of the vertical axis, and $\hat{\mathbf{e}}_{\mathbf{s}}$ is the unit vector along the flux tube.

Three steps are taken in order to get the initial conditions with one thread at each dip. First, we have a hydrostatic loop which is in an equilibrium state. Similar to Xia et al. (2011) and Zhang et al. (2013), the temperature (T) is a function of height (z) with the form

$$T(z) = T_1 + \frac{1}{2}(T_2 - T_1)(\tanh\left(\frac{z - h_0}{w_0}\right) + 1), \tag{6}$$

where $T_1 = 6000$ K is the temperature at the

chromosphere, whereas $T_2 = 1\,\mathrm{MK}$ is the temperature of the corona, $h_0 = 2.72$ Mm, and $w_0 = 0.25$ Mm. The density distribution is derived from the hydrostatic equilibrium equation (see Xia et al. 2011, for details). The background heating can also be derived, which balances the radiation. Second, we need to form two threads at the two dips. For that purpose, one way is to introduce symmetric heating localized in the chromosphere, which triggers chromospheric evaporation, and the ensuing condensation would naturally form threads at the dips, as demonstrated by Zhang et al. (2012, 2013). For simplicity, however, we form the threads in a straightforward way, i.e., by increasing the density by 2 orders of magnitude and decreasing the temperature by the same orders along two segments at the two dips. Each segment is chosen to be 20 Mm, which is the typical length for a filament thread (Engvold 2004). Note that the filament threads we get in this way are neither in hydrostatic equilibrium nor thermodynamic equilibrium. As the final step, we start the simulation to let the non-equilibrium state evolve and relax to an equilibrium state. This same method has been used in Terradas et al. (2015), and it is found to perform well.

Once the initial conditions with two segments of threads are determined, the threads are disturbed to oscillate. There are two types of perturbations, i.e., a momentum pulse or impulsive heating at one footpoint of the flux tube. According to Zhang et al. (2013), the oscillation properties are not sensitive to the perturbation type. Therefore, we choose to impose a velocity perturbation on the filament threads. As mentioned in §1, the perturbation might be due to a subflare near one footpoint of the magnetic field line (Jing et al. 2003) or due to a global coronal wave (Shen et al. 2014). In the former case, only one thread is perturbed initially; In the latter case, both threads would be perturbed quasi-simultaneously. In terms of the intrinsic magnetic geometry, the two dips can be similar or very different. Therefore, in this paper, we consider three cases: In case A, the two dips are identical, and the initial perturbation is imposed on one thread; In case B, the two dips are different, so the two threads have different intrinsic oscillation periods, and the initial perturbation is imposed on one thread; In case C, the two threads with different intrinsic oscillation periods are perturbed simultaneously. Another case with two identical dips and simultaneous perturbations can be ignored since the situation is equivalent to two separate threads.

The 1D radiative hydrodynamic equations are numerically solved with the MPI-Adaptive Mesh Refinement-Versatile Advection Code (MPI-AMRVAC, Keppens et al. 2012; Porth et al. 2014). In this work, we use 1200 initial grids with 7 levels of adaptive mesh refinement (AMR), which leads to an effective resolution ranging from 1.6 to 4.2 km in different cases. During the simulations, all the quantities are fixed at the boundaries (corresponding to the photosphere) since the dynamics in the corona has little influence on the two footpoints of the flux tube, as revealed by Xia et al. (2011), Luna et al. (2012), and Zhang et al. (2013).

3. Numerical Results

3.1. Case A: Active and passive threads on two identical dips

This is an ideal case where the two magnetic dips are identical, i.e., $w_1 = w_2 = l/2$, therefore, the intrinsic oscillation periods of the two threads are the same. The initial velocity perturbation is imposed on the first thread, which is called "active thread" hereafter. The velocity perturbation has the following form:

$$v(s) = \begin{cases} 0, & s < s_{1l} - \delta; \\ v_0(s - s_{1l} + \delta)/\delta, & s_{1l} - \delta \le s \le s_{1l}; \\ v_0, & s_{1l} \le s \le s_{1r}; \\ v_0(-s + s_{1r} + \delta)/\delta, & s_{1r} \le s \le s_{1r} + \delta; \\ 0, & s > s_{1r} + \delta; \end{cases} \tag{7}$$

where s_{1l} and s_{1r} are the left and right boundaries of the first filament thread, respectively; δ is the thickness of the transition layer which allows the velocity perturbation to vary smoothly along the flux tube. We set $w_1 = w_2 = l/2 = 80\,\mathrm{Mm}$, which are also comparable with previous works (Xia et al. 2011; Zhang et al. 2013; Zhou et al. 2014). It is noted that, as demonstrated by Zhang et al. (2013), the oscillation behavior is not sensitive to the form of perturbation. So the velocity profile can be chosen to be different from

equation (7), and the results would not be changed significantly.

Figure 2 displays the evolution of the temperature distribution along the flux tube, where the blue segments centered at $s = 63$ Mm and $s = 141$ Mm correspond to the two threads. It is seen that the first thread at $s = 63$ Mm (or active thread) starts to oscillate from the very beginning. As it moves, sound waves are excited, which propagate with a velocity of $116\,\mathrm{km\,s^{-1}}$ along the flux tube, as indicated by the arrows. When the first sound wave reaches the second thread (or passive thread) at $s = 141$ Mm, the passive thread starts to oscillate as well, but with a much smaller amplitude.

In order to study the oscillations more quantitatively, we trace the centers of the two threads at each time step. The evolutions of the thread centers are plotted in Figure 3 as dashed lines, where the top panel corresponds to the active oscillation of the first thread and the bottom panel corresponds to the passive oscillation of the second thread. It reveals that the active oscillation decays rapidly, whereas the passive oscillation is initially strengthened, gaining energy from the active thread, and then decays slowly. Similar to previous authors (Jing et al. 2003; Vršnak et al. 2007; Zhang et al. 2012), we fit the oscillations of the two threads with decayed sine functions:

$$\Delta s_1 = A_1 \mathrm{e}^{-t/\tau_1} \sin(\frac{2\pi}{p_1} t + \phi_1), \tag{8}$$

$$\Delta s_2 = A_2 \mathrm{e}^{-t/\tau_2} \sin(\frac{2\pi}{p_2} t + \phi_2), \tag{9}$$

where A, p, and ϕ are the amplitude, period, and phase of the oscillation, and the subscripts 1 and 2 refer to the oscillations of the first (active) and the second (passive) thread, respectively. Note that for the passive thread, its oscillation begins to damp after the second peak, i.e., since $t = 86$ min, hence the corresponding fitting starts at $t = 86$ min. The fitted curves are overplotted on Figure 3 as blue solid lines. It is seen that the oscillations of both threads are fitted very well by the decayed sine functions, with A_1=16.4 Mm, p_1=60 min, τ_1=89 min, and A_2=3.4 Mm, p_2=58 min, τ_2=230 min.

In order to check how these oscillation properties change with the geometry of the flux tube, we perform six other simulations with $l/2$ being 50 Mm, 60 Mm, 70 Mm, 90 Mm, 100 Mm, and 110 Mm. Such a range is chosen on purpose: If $l/2$ is too small, there would be direct exchange of materials between the two threads, whereas if $l/2$ is too large, the dips are too shallow so that the oscillations would deviate from the pendulum model controlled by gravity (Luna et al. 2012). The corresponding results are presented in Figure 4, where the red triangles represent the active thread, and the blue triangles represent the passive thread. Though not shown here, similar to $l/2 = 80$ Mm, the amplitudes of the active oscillations in these cases are 4–5 times larger than those of the passive oscillations. Whereas the oscillation periods are very close to each other, the damping timescale of the passive oscillation is generally 2–2.5 times longer than that of the active oscillation. In order to understand the effect of thread-thread interactions, we further perform simulations of a single-dipped flux tube, with the geometry of the magnetic dip, including the depth of the length, being the same as that of the active thread or passive thread. Note that since the damping timescale is also sensitive to the oscillation amplitude (Zhang et al. 2013), we keep the same oscillation amplitude for each corresponding simulation. The oscillation periods and the damping timescales in the single-dipped simulations are overplotted in Figure 4 as green circles (solid circles for the active thread and open circles for the passive thread). It is seen that the oscillation periods of both active and passive threads are close to those of the corresponding single-dipped simulations, and the damping timescales of the active oscillations are also close to the results of the single-dipped simulations, though slightly longer. However, the damping timescales of the passive oscillations are about 2.5–3 times longer than those of the single-dipped simulations.

3.2. Case B: Active and passive threads on two different dips

In observations, the two dips along one flux tube are probably not identical, with very different curvature radii. To construct a flux tube with non-identical dips, we take n in equation (5) to be 1.322, so that the length ratio of the two dips is $w_2/w_1 \approx 1.5$, which leads to the curvature radius of the second dip being twice that of the first dip. Note that the total length of the helix, l, is

adjusted in order to make sure that the curvature radius of the first dip (with a shorter length) in case B is the same as that in case A.

In this case, the same type of velocity perturbation is imposed on the first thread (or the active thread, the one in the shorter dip) as in case A. Similarly, in response to the sound waves excited by the active thread, the passive thread begins to oscillate, with an amplitude about 1/5 of the active oscillation. Similar to case A, both threads show damped oscillations, as revealed by Figure 5, which shows the evolutions of the temperature distributions in case B with $w_1 = 76$ Mm and $w_2 = 114$ Mm.

Again, we simulate six other cases with different lengths of the magnetic dips, and fit the oscillation profiles with the decayed sine functions as described by equations (8–9). The resulting periods and the damping timescales are displayed in Figure 6 as functions of the length of the dips. In this figure, the red triangles in the top row correspond to the active thread, and the blue triangles in the bottom row correspond to the passive thread. In order to check the effect of the thread-thread interaction, we also perform simulations of the single-dipped oscillations for both the active and passive threads. The corresponding results are represented by solid and open circles in Figure 6. It is found that for the active thread, the oscillation period is almost the same as in the single-dipped flux tube, with the difference becoming evident only when the length of the dip, w_1, is larger than 95 Mm, but the damping timescale is significantly smaller than that in the single-dipped case. The relative difference increases from 10% to 33% when w_1 increases from 47 Mm to 95 Mm. For the passive thread which has a larger length, w_2, both the oscillation period and the damping timescale deviate from the results of the single-dipped flux tube. It is seen that as the length of the dip, w_2, increases, the oscillation period becomes smaller and smaller than that in the single-dipped case. When w_2=156 Mm, the oscillation period drops by 16%. The variation of the damping timescale is remarkable, as indicated by Figure 6(d). Contrary to the case of a single-dipped flux tube where τ_2 decreases with w_2, the damping timescale of the passive thread in our case B increases with w_2 almost monotonically.

In the above simulations in this subsection, the velocity perturbation is imposed on the thread inside the shorter dip. It is therefore worth investigating the case with the initial perturbation imposed on the thread inside the longer dip. Note that the geometry of the flux tube is kept the same as in previous simulations in this subsection.

As shown in Figure 7, the passive thread (the thread in the shorter dip) starts to oscillate as a result of the sound waves excited by the active thread. The passive oscillation in this case has a slightly lower amplitude than the passive oscillation in Figure 5, which is about 1/6 of the amplitude of the active oscillation. Both threads experience a damped oscillation after the passive oscillation reached its peak at about $t = 53$ min.

Once again, we simulate six other cases with different lengths of the magnetic dips. Figure 8 displays the resulting periods and damping timescales as functions of the lengths of the dips. The symbols used here are the same as in Figure 6, but the subscript 1, corresponding to the first thread, represents the passive oscillations, and the subscript 2, corresponding to the second thread, represents the active thread. The green circles in Figure 8 also represent the results calculated from the single-dipped oscillations in order to check the effect of the thread-thread interaction. In contrast to the period of the passive oscillation in Figure 6, it is found that the oscillation periods of the passive thread in Figure 8(a) are almost the same as those of the single-dipped case. However, the oscillation periods of the active thread in Figure 8(c) are about 1/4 smaller than those of the single-dipped case. The damping timescale of the the passive threads in Figure 8(b) shows a tendency similar to the passive thread in Figure 6(d), i.e., τ increases with increasing w almost monotonically. However, the damping timescales of the active thread in Figure 8(d) are 60–70% longer than those in the single-dipped cases, which is opposite to the situation in Figure 6(b).

3.3. Case C: Non-uniform helix with concurrent perturbations

In this case, the geometry of the helix is the same as in case B, but the same velocity perturbation as described by equation (7) is also imposed on the second thread simultaneously. Note that s_{1l} and s_{1r} are replaced with s_{2l} and s_{2r} for the second thread.

The dashed lines in Figure 9 describe the oscillations of the two threads in the case with w_1=76 Mm and w_2= 114 Mm, where the top panel corresponds to the thread with a shorter dip and the bottom panel corresponds to the thread with a longer dip. It is seen that whereas the oscillation of the second thread (with the length of dip w_2) can be well fitted with a decayed sine function, the oscillation of the first thread (with the length of dip w_1) decays rapidly in the first two periods, and then keeps almost the same amplitude like a decayless oscillation. The profile can be fitted neither with a decayed sine function nor a decayed Bessel function which was used to describe large-amplitude longitudinal oscillations by Luna & Karpen (2012). Therefore, we use the decayed sine functions to fit all the simulation data for the second thread and the early data (i.e., in the first two periods) for the first thread. The fitted functions are overplotted in Figure 9 as blue curves.

Similar to cases A and B, we perform other simulations with different lengths of the magnetic dips. Figure 10 displays how the fitted periods and damping timescales change with the length of the dips. We can see that for the first thread (top row), the oscillation periods (red triangles) are 14–20% higher than those in the single-dipped flux tube (green solid circles). Its initial damping timescales during the first two periods (red triangles) are remarkably smaller than those in the single-dipped flux tube (green solid circles). For the second thread (bottom row), the oscillation periods are roughly the same as in the single-dipped flux tube (only when w_2 becomes large, the discrepancy becomes significant). However, the damping timescales (blue triangles) are significantly larger than those in the single-dipped situation (green open circles).

4. Discussions

Waves or oscillations carry important information about the local magnetic field and/or plasma, and both the oscillation period and the damping timescale can be used to diagnose the thermal and magnetic structures in the corona (Andries et al. 2009). The same as other types of waves or oscillations, the large-amplitude longitudinal oscillations of solar filaments have also been applied to derive the magnetic properties of the filaments (Luna & Karpen 2012; Zhang et al. 2013). However, all the previous simulation work was based on the assumption that there is only one filament thread along each magnetic field line. Either from theoretical or extrapolation points of view, some magnetic field lines may have two or more dips, supporting two or more threads along one flux tube. In this case, the oscillation of each thread is not independent, and the interactions between the threads are expected to change the oscillation behaviors of each thread. With 1D radiative hydrodynamic simulations of the oscillations of two threads along one flux tube, we showed that indeed the oscillation properties are changed a lot, compared to the case of a single-dipped flux tube.

For the special case where the two dips are identical and one thread is perturbed initially (i.e., case A), energy is transferred from the active thread to the passive thread, as indicated by the temperature front which is marked by the arrows in Figure 2. As a result, the oscillation of the passive thread decays very slowly, with the damping timescale 2–2.5 times longer than in the case of a single-dipped flux tube. The decay of the oscillation of the active thread is not much affected. This is understandable since only 4% of its energy is transferred to the passive thread, as implied by the ratio of the amplitudes of the active and passive threads being about 5. It is also noticed that although the oscillation of the passive thread is delayed initially with respect to the active thread due to limited propagation velocity of sound waves, the oscillation of the two threads tend to be synchronous as implied by the fifth peaks of both oscillations in Figure 3. This means that the interaction between the two threads leads to the synchronization of their oscillations.

In the case where the curvature radius of the passive thread is twice that of the active thread, it seems that the oscillation period of the thread inside the shorter dip is barely affected by the thread-thread interaction, no matter it is active or passive oscillation. However, for the thread inside the longer dip, its oscillation period is significantly reduced, i.e., by 26% when compared to the single-dipped case, especially when it is the active thread. Only when its length is below 100 Mm and it is the passive thread, the oscillation period is not affected by the thread-thread inter-

action. This is probably because the gas pressure gradient overtakes the field-aligned gravity when the length of the dip is large, as demonstrated by Luna et al. (2012). The short-period oscillation of the shorter thread continues to excite sound waves, which serve as the external driving force for the longer thread, making the oscillation period of the latter closer to the period of the shorter thread. The modification of the damping timescale is remarkable. Its variation with the length of the magnetic dip depends strongly on whether it is the active or passive thread. For the active thread, its damping timescale (τ) decreases with the increasing length of the magnetic dip, the same as in the single-dipped case, though τ may be reduced or increased in comparison to the single-dipped case, depending on whether the magnetic dip is shorter or longer; For the passive thread, its damping timescale (τ) increases with the increasing length of the magnetic dip, completely opposite to the single-dipped case.

There are various types of perturbations in the dynamic solar corona, including the ceaseless convection motions or p-mode oscillation near the solar surface, trapped waves from solar flares (Liu et al. 2012), global coronal waves driven by coronal mass ejections (Chen 2009). If it is due to a nearby subflare (Vršnak et al. 2007), one segment of thread is triggered to oscillate, which would drive another magnetically-connected segment of thread to oscillate, as discussed above. However, when a global coronal wave sweeps the filament (Liu et al. 2012; Shen et al. 2014), both segments would be triggered to oscillate nearly simultaneously. Our simulations of such a case indicate that the oscillation period of the thread with a smaller curvature radius (hence shorter period) becomes 15–20% larger, whereas the oscillation period of the thread with a larger curvature radius (hence longer period) is reduced slightly. The oscillation of the first thread decays rapidly in the first two periods, and then experiences a decayless stage thereafter. It means that kinetic energy of the thread with a smaller curvature radius is initially transferred significantly to the other thread, leading to the strong damping of itself and the slow damping of the other thread with a larger curvature radius. In the later stage, it seems that kinetic energy is transferred back to the first thread, leading to a decayless oscillation of the first thread.

It has been proposed that both the oscillation period and the damping timescale can be utilized for consistent seismology (see Arregui et al. 2012, for a review). In terms of longitudinal oscillations of solar filaments, Zhang et al. (2013) have done a parameter survey and derived empirical formulae to relate the oscillation period and damping timescale to the geometric parameters of the magnetic dips. Based on the simulations in this paper, it becomes clear that we have to be careful when applying the empirical formulae to observations, especially when one thread is magnetically connected to another thread. The results of this paper can be summarized as follows: It seems that the period of filament longitudinal oscillation is not affected too much by the interaction between two threads, except the case of the active thread inside the longer dips, where the gas pressure gradient becomes unnegligible (Luna et al. 2012). Even in the latter case, the oscillation period is reduced by only 26% compared to the case of a single-dipped flux tube. However, the situation of the damping timescale is complex, which might be modified significantly by the interaction between magnetically-connected threads. When the two dips are identical (or similar) and only the active thread is perturbed initially, the damping timescale of the active thread is changed significantly, which decreases by 25% if the active thread has a shorter magnetic dip and increases by 75% if the active thread has a longer dip. More importantly, the thread-thread interaction completely changes the behavior of the damping timescale of the passive thread, which increases with the increasing length of the magnetic dip, a result opposite to the case of a single-dipped flux tube. When the two threads on non-identical dips are perturbed simultaneously, the oscillation of the thread with a shorter period cannot be described by a decayed sine function nor a decayed Bessel function. It decays drastically during the first two periods, and then becomes kind of decayless. The thread with a longer period, however, can be well fitted with a decayed sine function, with the damping timescale increased owing to the thread-thread interaction.

It is noted here that the results presented in this paper are based on a simple model, with two segments of filament threads situated at two magnetic dips along one rigid flux tube. All the con-

clusions are worthy to be verified in future by two- or three-dimensional simulations.

ZYH thanks Mr. T. Shi from University of Michigan for his help with scripting in Adobe® Photoshop® CC. The numerical calculations in this paper were performed on the cluster system in the High Performance Computing Center (HPCC) of Nanjing University. This research was supported by the Chinese foundations (NSFC 11533005 & 11025314) and Jiangsu 333 Project.

REFERENCES

Andries, J., van Doorsselaere, T., Roberts, B., et al. 2009, Space Sci. Rev., 149, 3

Antiochos, S. K., MacNeice, P. J., & Spicer, D. S. 2000, ApJ, 536, 494

Antiochos, S. K., MacNeice, P. J., Spicer, D. S., & Klimchuk, J. A. 1999, ApJ, 512, 985

Arregui, I., Oliver, R., & Ballester, J. L. 2012, Living Reviews in Solar Physics, 9, 2

Aschwanden, M. J., & Schrijver, C. J. 2002, ApJS, 142, 269

Bashkirtsev, V. S., Kobanov, N. I., & Mashnich, G. P. 1983, Sol. Phys., 82, 443

Chen, P. F. 2009, ApJ, 698, L112

Chen, P. F., Harra, L. K., & Fang, C. 2014, ApJ, 784, 50

Díaz, A. J., Oliver, R., & Ballester, J. L. 2005, A&A, 440, 1167

Díaz, A. J., & Roberts, B. 2006, Sol. Phys., 236, 111

Engvold, O. 2004, in IAU Symposium, Vol. 223, Multi-Wavelength Investigations of Solar Activity, ed. A. V. Stepanov, E. E. Benevolenskaya, 187

Erdélyi, R., & Fedun, V. 2007, Science, 318, 1572

Jing, J., Lee, J., Spirock, T. J., et al. 2003, ApJ, 584, L103

Jing, J., Yuan, Y., Wiegelmann, T., et al. 2010, ApJ, 719, L56

Joarder, P. S., & Roberts, B. 1992a, A&A, 256, 264

—. 1992b, A&A, 261, 625

Karpen, J. T., Antiochos, S. K., Hohensee, M., Klimchuk, J. A., & MacNeice, P. J. 2001, ApJ, 553, L85

Karpen, J. T., Antiochos, S. K., & Klimchuk, J. A. 2006, ApJ, 637, 531

Karpen, J. T., Tanner, S. E. M., Antiochos, S. K., & DeVore, C. R. 2005, ApJ, 635, 1319

Keppens, R., Meliani, Z., van Marle, A. J., et al. 2012, Journal of Computational Physics, 231, 718

Kippenhahn, R., & Schlüter, A. 1957, ZAp, 43, 36

Li, T., & Zhang, J. 2012, ApJ, 760, L10

Lin, Y., Engvold, O., Rouppe van der Voort, L. H. M., & van Noort, M. 2007, Sol. Phys., 246, 65

Liu, W., Ofman, L., Nitta, N. V., et al. 2012, ApJ, 753, 52

Luna, M., Díaz, A. J., & Karpen, J. 2012, ApJ, 757, 98

Luna, M., & Karpen, J. 2012, ApJ, 750, L1

Luna, M., Terradas, J., Khomenko, E., Collados, M., & de Vicente, A. 2016, ApJ, 817, 157

Mackay, D. H., & van Ballegooijen, A. A. 2009, Sol. Phys., 260, 321

Martens, P. C., & Zwaan, C. 2001, ApJ, 558, 872

Oliver, S., Mann, R. G., Carballo, R., et al. 2002, MNRAS, 332, 536

Porth, O., Xia, C., Hendrix, T., Moschou, S. P., & Keppens, R. 2014, ApJS, 214, 4

Ramsey, H. E., & Smith, S. F. 1966, AJ, 71, 197

Shen, Y., Ichimoto, K., Ishii, T. T., et al. 2014, ApJ, 786, 151

Soler, R., Arregui, I., Oliver, R., & Ballester, J. L. 2010, ApJ, 722, 1778

Tandberg-Hanssen, E., ed. 1995, Astrophysics and Space Science Library, Vol. 199, The nature of solar prominences

Terradas, J., Molowny-Horas, R., Wiehr, E., et al. 2002, A&A, 393, 637

Terradas, J., Soler, R., Oliver, R., & Ballester, J. L. 2015, ApJ, 802, L28

Vršnak, B., Veronig, A. M., Thalmann, J. K., & Žic, T. 2007, A&A, 471, 295

Wang, Y.-M., & Sheeley, Jr., N. R. 1999, ApJ, 510, L157

Withbroe, G. L. 1988, ApJ, 325, 442

Withbroe, G. L., & Noyes, R. W. 1977, ARA&A, 15, 363

Xia, C., Chen, P. F., Keppens, R., & van Marle, A. J. 2011, ApJ, 737, 27

Yi, Z., Engvold, O., & Keil, S. L. 1991, Sol. Phys., 132, 63

Zhang, Q. M., Chen, P. F., Xia, C., & Keppens, R. 2012, A&A, 542, A52

Zhang, Q. M., Chen, P. F., Xia, C., Keppens, R., & Ji, H. S. 2013, A&A, 554, A124

Zhang, Y., & Engvold, O. 1991, Sol. Phys., 134, 275

Zhou, Y.-H., Chen, P.-F., Zhang, Q.-M., & Fang, C. 2014, Research in Astronomy and Astrophysics, 14, 581

Zou, P., Fang, C., Chen, P. F., Yang, K., & Cao, W. 2017, ApJ, 836, 122

Zou, P., Fang, C., Chen, P. F., et al. 2016, ApJ, 831, 123

This 2-column preprint was prepared with the AAS LaTeX macros v5.2.

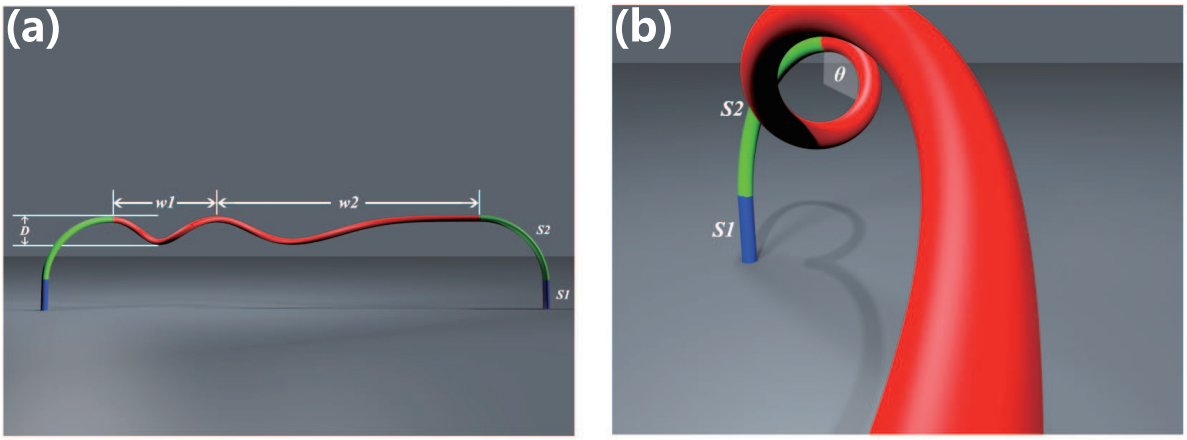

Fig. 1.— (a) The front view and (b) The side view of the magnetic field configuration used in our work. Different colors represent segments described with different equations. Note that there are two magnetic dips in the displayed magnetic field line, and two separate threads are formed at the two dips.

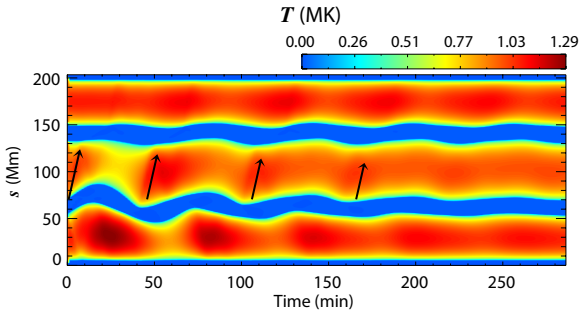

Fig. 2.— Evolution of the temperature distribution along the magnetic flux tube in case A after the velocity perturbation is imposed on the thread centred at 63 Mm. Black arrows represents energy transfer done by sound waves.

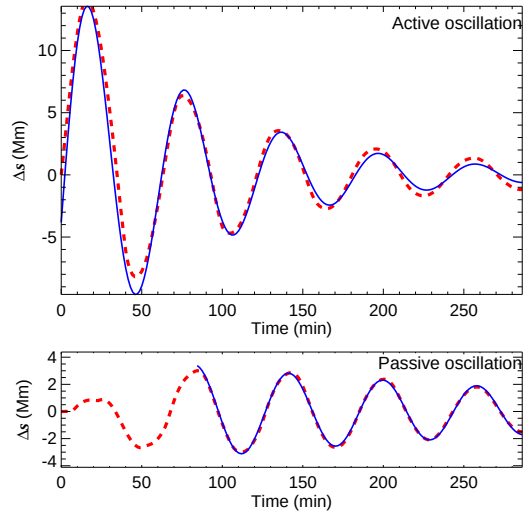

Fig. 3.— Oscillations of the two filament threads in case A, with the upper panel for the first (active) thread and the lower panel for the second (passive) thread, respectively. The red dashed curves are the spatial displacement of the mass centres of the two filament threads in our numerical simulations, and the blue solid lines are the fitting curves generated by the decayed sine functions.

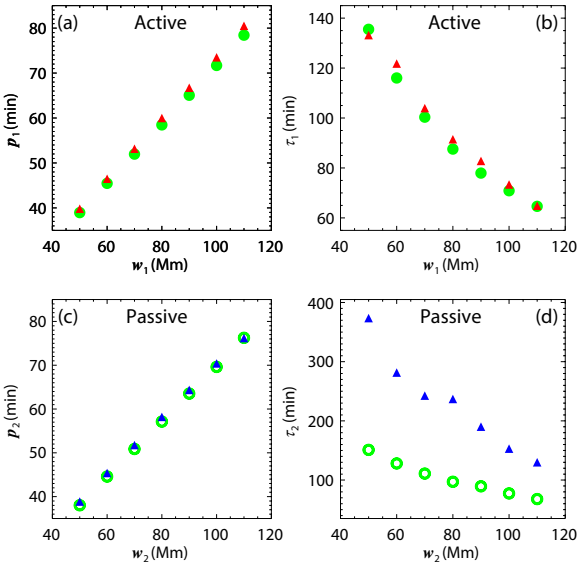

Fig. 4.— Scatter plots of the period (panel a) and the damping timescale (panel b) of the active thread (*red triangles*) in case A; Scatter plots of the period (panel c) and the damping timescale (panel d) of the passive thread (*blue triangles*) in case A. Green (solid and open) circles are the results from the corresponding single-dipped simulations.

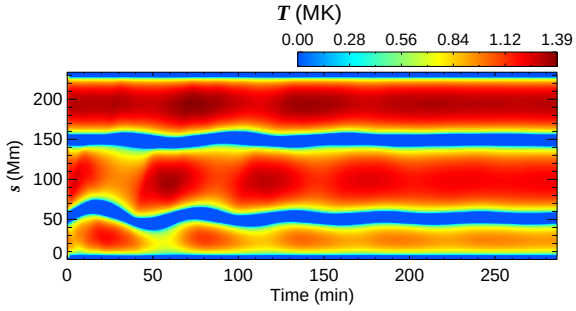

Fig. 5.— Evolution of the temperature distribution along the magnetic flux tube in case B after the velocity perturbation is imposed on the thread centred at s =52 Mm.

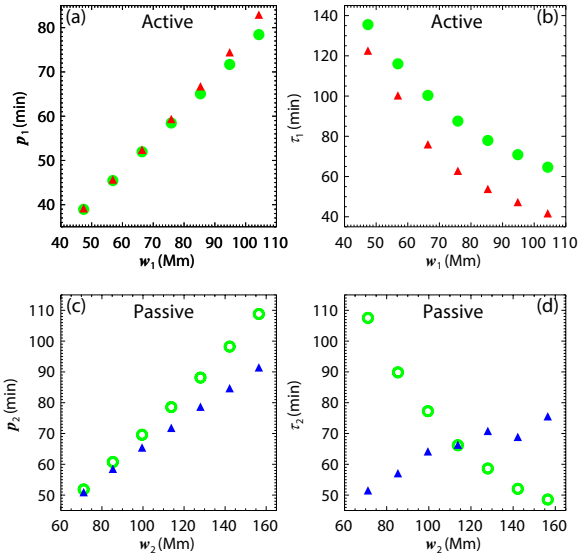

Fig. 6.— Scatter plots of the period (panel a) and the damping timescale (panel b) of the active thread (*red triangles*) in case B; Scatter plots of the period (panel c) and the damping timescale (panel d) of the passive thread (*blue triangles*) in case B. Green (solid and open) circles are the results from the corresponding single-dipped simulations.

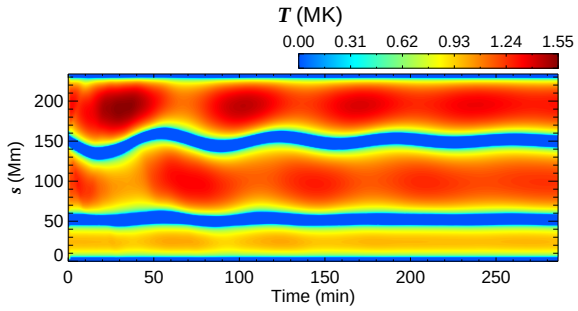

Fig. 7.— Evolution of the temperature distribution along the magnetic flux tube in case B after the velocity perturbation is imposed on the thread centred at s =152 Mm.

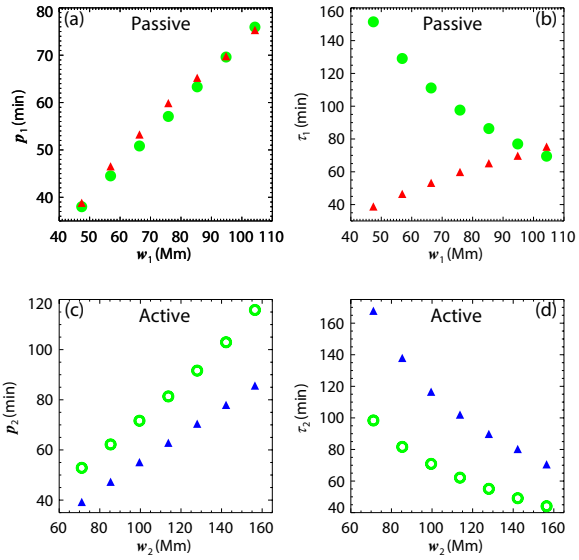

Fig. 8.— The same as Fig. 6, but the active thread where the initial perturbation is imposed is the one at the longer magnetic dip.

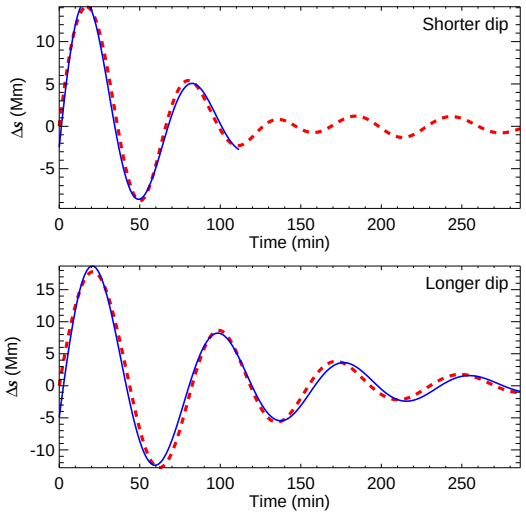

Fig. 9.— Oscillations of the two filament threads in case C, with the upper panel for the thread at the shorter magnetic dip and the lower panel for the thread at the longer dip, respectively. The red dashed curves are the spatial displacement of the mass centres of the two filament threads in our numerical simulations, and the blue solid lines are the fitting curves generated by the decayed sine functions.

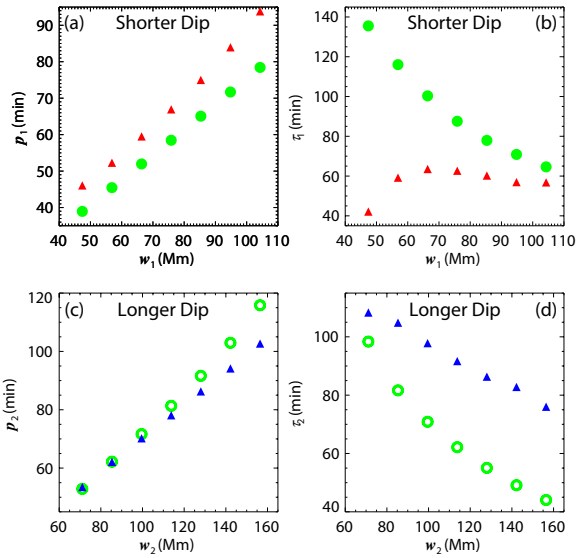

Fig. 10.— Scatter plots of the period (panel a) and the damping timescale (panel b) of the thread at the shorter magnetic dip (*red triangles*) in case C; Scatter plots of the period (panel c) and the damping timescale (panel d) of the thread at the longer dip (*blue triangles*) in case C. Green (solid and open) circles are the results from the corresponding single-dipped simulations.